PRJ, Vol. 7 (January 1995); P. 35–41, 13 FIGS, 1 TABLE.

FRACTOGRAPHY EXHIBITED BY HYDROGEN EMBRITTLED AUSTENITIC STAINLESS STEELS

F.O. El-Shawesh*

أثر التصلد الهيدروجيني على التغير في طبيعة الكسر للفولاذ الأوستيني قليل الصداء

فوزي الشاوش

تم شحن عينات من الفولاذ قليل الصداء ، الأولى من نوع 304 في حالة ملدنة ومدرفلة وفي حالة حساسة (Sensitization) نتيجة ترسب الكربيدات ($C_{23}C_6$) في حدود الحبيبات والثانية في حالة ملدنة ومن نوع 310 ، بالهيدروجين عند درجة حرارة الغرفة وفي محلول مائي $1N\text{-}H_2SO_4$ مضاف إليه قليل من صوديوم ساينيد كعامل مساعد في إنتشار الهيدروجين في الصلب . تم عملية شحن العينات وهي معرضة لإجهادات شد بطيئة وبسرعات مختلفة (833.3 nm/s إلى 9.8 nm/s).

في حالة الصلب قليل الصداء نوع 304 أظهرت النتائج أن الكسر إنتشر خلال وعبر الحبيبات عند إجهادات شد بطيئة جداً (9.8 nm/s و83.3 nm/s) ، كما لوحظ أن معدل الكسر خلال الحبيبات يزداد بانخفاض سرعة الشد البطيئ . نفس ميكانيكية الكسر لوحظت في العينات المدرفلة من نوع 304 إلا أن معدل الكسر خلال الحبيبات كان أقل .

عينات الفولاذ من نوع 304 والتي حدود حبيباتها تحتوي على ($Cr_{23}C_6$) إعتمدت ميكانيكية الكسر فيها على زمن المعالجة الحرارية والسرعة المستخدمة في إجهاد الشد البطيئ . الكسر في عينات الصلب قليل الصداء في نوع 310 كان خلال وعبر الحبيبات وذلك عند تطبيق أجهاد الشد البطيئ جداً (9.8 nm/s) .

ABSTRACT

Annealed, sensitized and cold worked less stable 304 austenitic stainless steel and more stable 310 austenitic stainless steel in annealed condition were cathodically charged in 1N H_2SO_4 with addition of $NaAsO_2$ at current density of 0.4 mA/cm^2 while undergoing tensile strain over a wide range of crosshead speeds (833.3 nm/s to 9.8 nm/s) at room temperature.

Fracture surface of 304 austenitic stainless steel specimens exhibited both cleavage and intergranular fracture at low crosshead speeds of 83.3 nm/s and 9.8 nm/s. The extent of intergranular fracture was observed to increase with lowering in crosshead speed. Similar features were observed when cold worked 304 austenitic stainless steel specimens tested at the same condition. However, the extent of intergranular fracture was less compared to the non cold worked specimens.

Fracture surface of sensitized 304 austenitic stainless steel specimens exhibited different surface morphology and was found to depend on the sensitization time and the applied crosshead speed.

Both intergranular and quazi cleavage types of fracture modes were observed when stable 310 austenitic stainless steel specimens tested at the lowest corsshead speed of 9.8 nm/s.

INTRODUCTION

Ductility of many austenitic stainless steel is reduced by charging with hydrogen or by testing in a hydrogen atmosphere [1–4]. Embrittlement is substantial with ductility losses of up to 50% or higher, when 304 austenitic stainless steel is tested in high pressure hydrogen [1], strained while undergoing cathodic charging and when tensile tested after severly charged by hydrogen [1, 5]. Other varieties of austenitic stainless steel, such as type 310 austenitic stainless steel, is affected slightly under the same condition [3]. Explanation for the relatively high susceptibility of type 304 austenitic stainless steel to

*Petroleum Research Centre, P.O. Box 6431, Tripoli, G.S.P.L.A.J.

hydrogen embrittlement was attributed to the strain induced transformation to α-martensite [1, 2] or concentration of hydrogen at critical site by coplanar dislocation motion [6, 7].

Changes in fracture morphology have been observed in tensile specimens tested in hydrogen. Microvoid formation and coalescence leading to a dimpled fracture is the only fracture mode observed in hydrogen free type of 304 and 310 austenitic stainless steels [8, 9]. In contrast, fracture referred to as cleavage fracture [10] quazi cleavage [11, 12], intergranular fracture [2, 13, 14, 15], facets [16] have been reported for hydrogen embrittlement of 304 austenitic stainless steel. However, microvoid coalescence was the predominant fracture morphology for 310 austenitic stainless steel [8, 10].

This paper discusses the effect of strain rate (crosshead speed), microstructure and stability on the changes in the fracture morphology for less stable 304 and more stable 310 types of austenitic stainless steels as a result of hydrogen embrittlement.

EXPERIMENTAL

A commercial 304 and 310 austenitic stainless steel were used for this course of work. These alloys were selected in order to investigate the effect of different alloy stabilities on susceptibility to hydrogen embrittlement. The alloy 304 was selected because its austenite phase is less stable and would be expected to transform to both α and ε phases under either subzero cold working or cathodic charging. In the 310 alloy the austenite phase is anticipated to be highly stable. The chemical composition for these alloy steels are shown in Table 1. The samples were solution annealed at 1050 °C for 304 austenitic stainless steel and at 1100 °C for 310 austenitic stainless steel for 1 h followed by water quench. Some samples from 304 austenitic stainless steel were given an additional heat treatment (sensitization) at 650 °C for duration of 5 h and 24 h. This treatment cause chromium carbide ($Cr_{23}C_6$) to precipitate at the grain boundaries as a result of chromium and carbon depletion from the area adjacent to the grain boundaries.

A number of 304 austenitic stainless steel samples were cold worked up to 12% in order to examine the susceptibility of cold worked structure to the hydrogen embrittlement.

Table 1. Chemical Composition of the 304 and 310 Austenitic Stainless Steels

Materials	C%	Mn%	Si%	P%	S%	Cr%	Ni%
304	0.04	1.42	0.32	0.024	0.002	18.36	8.73
310	0.026	1.52	0.27	0.013	0.005	24.66	20.07

The material was received in the form of sheet with thickness of 0.8 mm. The specimens was then machined to required dimension and 60° V notch as introduced at the middle as shown in Fig. 1. All test specimens were tensile strained while undergoing cathodic charging at current density of 0.4 mA/cm² in 1*N* H_2SO_4 with addition of $NaAsO_2$ at room temperature. For comparison the same number of specimens were tested in air. The resulted fracture surfaces were cleaned in acetone using ultrasonic and then dried. A scanning electron microscope (SEM) was then used to examine the changes in the fracture morphology as a result of hydrogen embrittlement.

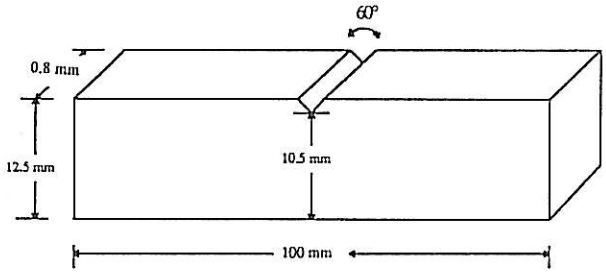


FIG. 1. Schematic representation showing the shape and dimensions (mm) of the type of specimen used in the hydrogen embrittlement test.

FRACTOGRAPHY

Three features were observed on the fracture surfaces of the tested specimens: dimples, cleavage and intergranular. Dimpled rupture was the only fracture mode observed on the specimens tested in air as shown in Fig. 2. The other two fracture modes were found only in specimens that were embrittled as a result of absorbed hydrogen.

The results will be classified into three main sections in order to clarify the different effects.

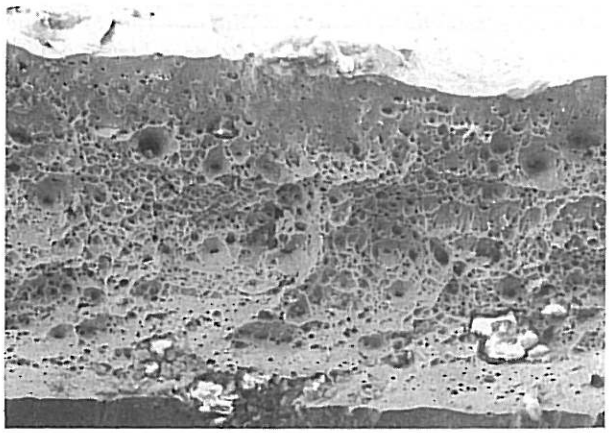


FIG. 2. S.E.M. fractography shows typical ductile fracture of stainless steel specimen fractured in air.

1. Effect of sensitization

Sensitized 304 austenitic stainless steel specimens exhibited higher susceptibility to hydrogen embrittlement compared when it is in the annealed condition. The degree of the susceptibility was found to depend on the sensitization time and used crosshead speed. The fracture surfaces for specimens sensitized for 24 h was predominantly intergranular particularly at two lowest crosshead speeds of 83.3 nm/s and 9.8 nm/s as shown in Fig. 3. The percentage of intergranular fracture was found to increase with lowering in crosshead speed. However, at these crosshead speed, cleavage fracture was predominant fracture mode for specimens sensitized for only 5 h as shown in Fig. 4.

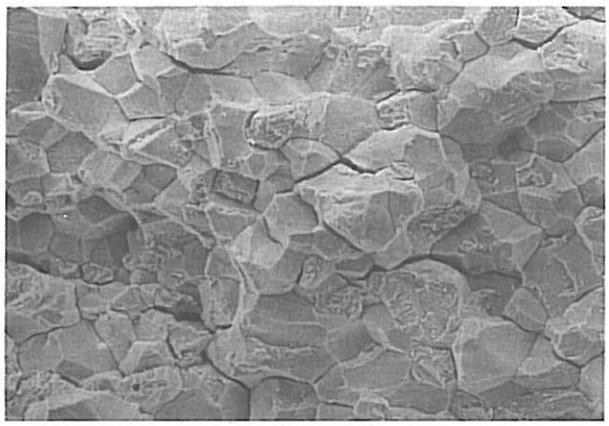


FIG. 3. S.E.M. fractograph of a 24 h sensitized 304 austenitic stainless steel specimen strained in solution at a crosshead speed of 9.8 nm/s. Fractograph shows faceted intergranular and little transgranular cleavage fracture.



FIG. 4. S.E.M. fractograph of a 5 h sensitized 304 austenitic stainless steel specimen strained in solution at a crosshead speed of 9.8 nm/s. Fractograph shows transgranular cleavage and little intergranular fracture.

2. Effect of cold work

Cold worked 304 austenitic stainless steel specimens exhibited pronounced embrittlement at lower crosshead speeds of (833.3 nm/s to 9.8 nm/s). The resulted fracture surfaces exhibited similar features to that observed for annealed specimens as shown in Fig. 5. Little ductile tearing was observed at the middle of fracture surface for specimens tested at the lowest crosshead speed of 9.8 nm/s.

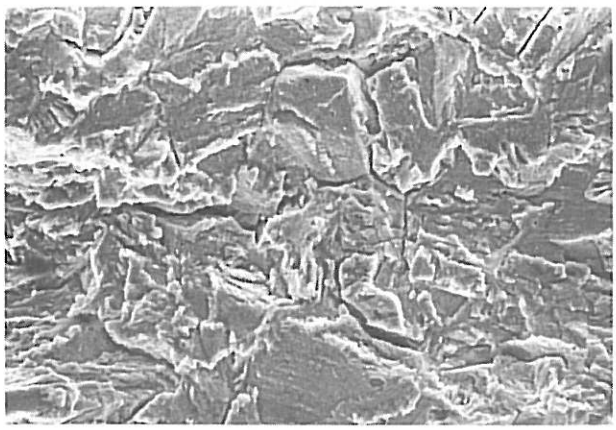


FIG. 5. S.E.M. fractograph of an 12% cold worked 304 austenitic stainless steel specimen strained in solution at a crosshead speed of 83.3 nm/s. Fractograph show both cleavage fracture and some intergranular fracture. Isolated areas of ductile tearing are observed.

3. Effect of stability

This section will show the effect of hydrogen on the two different stability austenitic stainless steels respectively less stable 304 and more stable 310 austenitic stainless steels. The degree of embrittlement was observed to increase with decreasing in crosshead speed and stability of the tested alloy. Less stable 304 austenitic stainless steel exhibited transgranular cleavage fracture and little intergranular fracture at low crosshead speeds (833.3 nm/s–83.3 nm/s) as shown in Fig. 6. Mixed mode transgranular cleavage fracture and faceted intergranular fracture was ob-

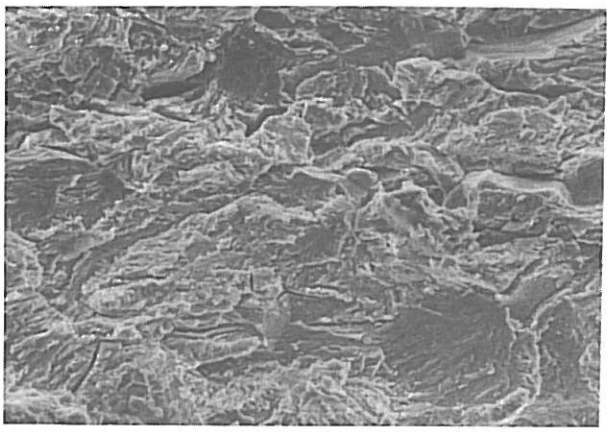


FIG. 6. S.E.M. fractograph of a 304 austenitic stainless steel specimen strained in solution at crosshead speed of 83.3 nm/s. Fractograph show cleavage fracture and some intergranular fracture.

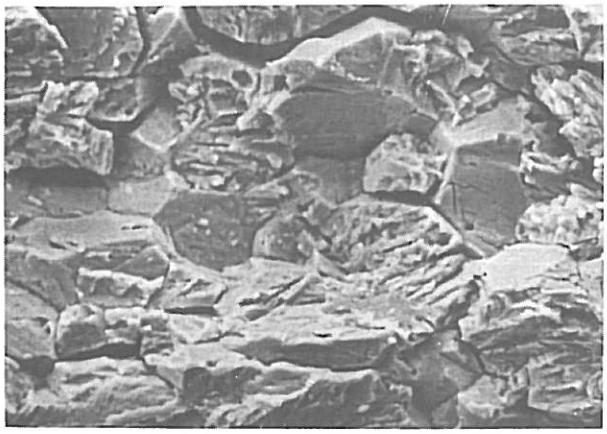


FIG. 7. S.E.M. fractograph of a 304 austenitic stainless steel specimen strained in solution at a crosshead speed of 9.8 nm/s. Fractograph show faceted intergranular fracture and some transgranular cleavage fracture.

served at the lowest crosshead speed of 9.8 nm/s as shown in Fig. 7. This faceted intergranular fracture was not reported earlier.

The more stable 310 austenitic stainless steel, which have high stacking fault energy (SFE) compare to less stable 304 austenitic stainless steel, shows less susceptibility to hydrogen embrittlement which is manifested in little changes in fracture morphology when only tested at the lowest crosshead speed of 9.8 nm/s. The change in fracture morphology was observed to be restricted at the areas in which high stress concentration attained e.g. notch and specimen edges. Both intergranular and quazi cleavage types of fracture modes were observed at these areas as shown in Figs. 8 and 9. This type of fracture was not reported earlier for this type of steel.

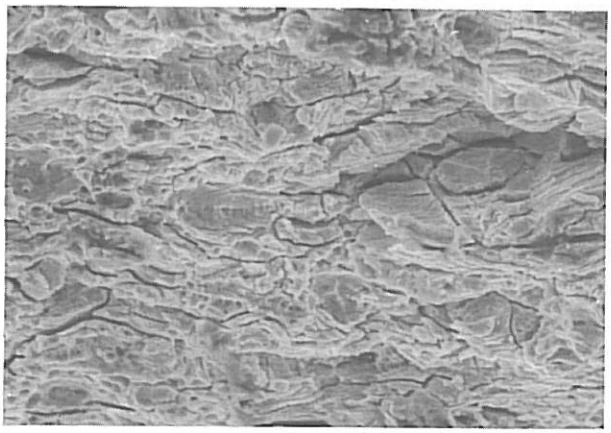


FIG. 8. S.E.M. fractograph of a 310 austenitic stainless steel specimen strained in solution at a crosshead speed of 9.8 nm/s. Fractograph shows details of fracture in the middle of the specimens, where quazi cleavage fracture and some intergranular fracture were visible.

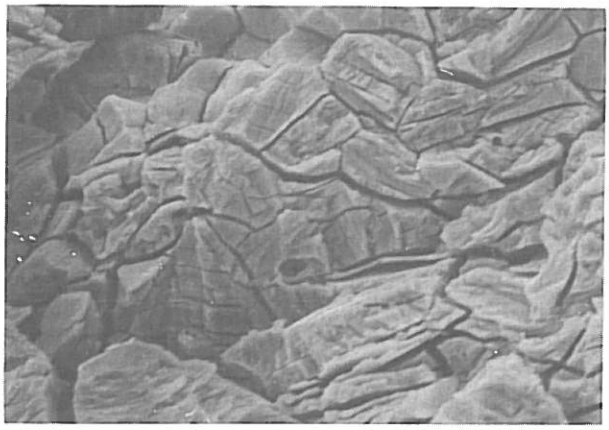


FIG. 9. S.E.M. fractograph of a 310 austenitic stainless steel specimen strained in solution at a crosshead speed of 9.8 nm/s. Fractograph show details of fracture at the specimen edge, where intergranular fracture and quazi cleavage fracture are visible.

SURFACE CRACK

Surface cracks on the surface of hydrogen embrittled less stable 304 austenitic stainless steel specimens in annealed, sensitized and cold worked condition and more stable 310 austenitic stainless steel specimens in annealed condition are shown respectively in Fig. 10–13. Both intergranular and transgranular cracks were observed on the surfaces of these tested specimens. Some of transgranular cracks were observed to propagate along or parallel to the slip bands as shown in Fig. 10 for 304 austenitic stainless steel specimens in annealed condition. Cold worked specimens exhibited less surface cracks compared to the annealed specimens as shown in Fig. 11. Sensitized specimens showed more transgranular cracks

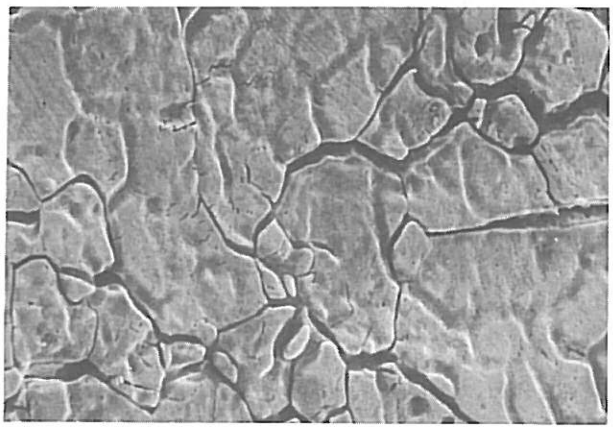


FIG. 10. S.E.M. micrograph of the surface of a 304 austenitic stainless steel specimen strained in solution at a crosshead speed of 9.8 nm/s. Micrograph show intergranular and many transgranular cracks. Some of transgranular cracks are appeared to be parallel to the slip bands.



FIG. 11. S.E.M. micrograph of an 12% cold worked 304 austenitic stainless and specimen strained in solution at a crosshead of 9.8 nm/s. Micrograph shows very little surface cracks.

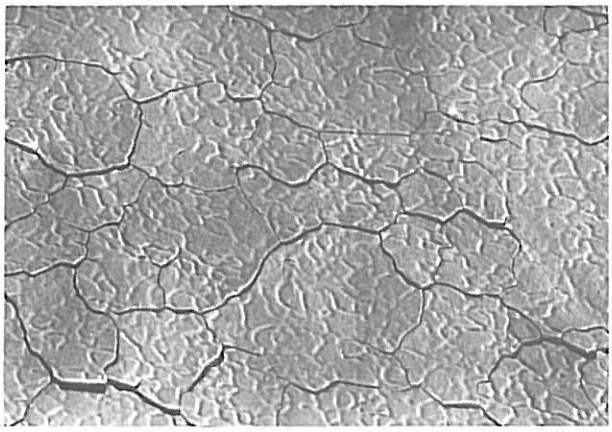


FIG. 12. S.E.M. micrograph of a 5 h sensitized 304 austenitic stainless steel specimens strained in solution at a crossheadspeed of 9.8 nm/s. Micrograph shows both transgranular and intergranular cracks.

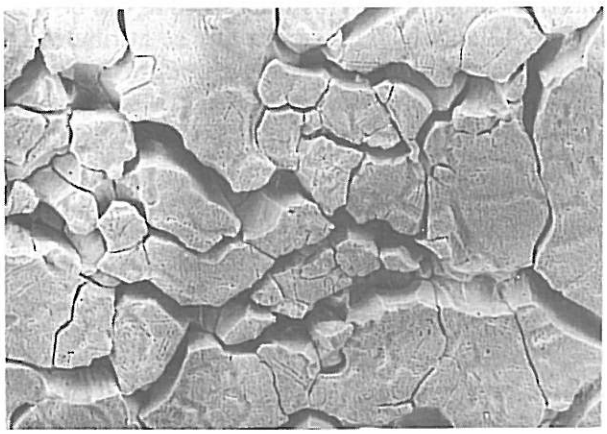


FIG. 13. S.E.M. micrograph of a 24 h sensitized 304 austenitic stainless steel specimen strained in solution at a crosshead speed of 9.8 nm/s. Micrograph show deep intergranular cracks and grain spall off. Transgranular cracks are visible.

compared to that observed for annealed specimens as shown in Fig. 12. Grain spall off was observed in specimens sensitized for 24 h as shown in Fig. 13. The extent of surface cracking for sensitized specimens was observed to increase with increasing in sensitizing time.

DISCUSSION

It is clear that the results naturally group themselves by heat treatment. If samples are aged (sensitized), the fracture mode is predominantly intergranular [13, 14, 15]. If the samples are only solution annealed, the crack usually proceeds along a transgranular path [10]. The intergranular fracture of sensitized specimens was attributed to the chromium depletion at the grain boundaries [13, 14]. This depletion makes the material at the grain boundaries, less stable, much more susceptible to α-martensite formation [14]. Since the martensite is much susceptible to hydrogen cracking, intergranular fracture occurs [14]. One should also note that martensite forms, at the grain boundaries, a continuous path for easy cracking through the sample [9]. This continuity is far more important than the volume percent of martensite [14].

The above discussion is in agreement with the observation of intergranular fracture only in the specimens sensitized for 24 h as shown in Fig. 2. Transgranular cleavage fracture was the predominant fracture mode for 5 h sensitized specimens. This results can be attributed to the less or/and non continuous martensite formation in 5 h sensitized specimens. Short sensitization time leads to less chromium depletion which in turn results in less martensite formation.

Faceted intergranular fracture was observed as well in the solution annealed 304 austenitic stainless steel specimens tested in hydrogen at the lowest crosshead speed of 9.8 nm/s as shown in Fig. 7. This result can be attributed mainy to the high hydrogen concentration at the grain boundaries as a result of dislocation bearing hydrogen piled-up at these boundaries [10]. Such clear faceted intergranular fracture was not reported before and may be produced as a result of using a very slow crosshead speed of 9.8 nm/s in this work which allow high hydrogen concentration to be attained.

Transgranular cleavage was observed in annealed and cold worked less stable 304 austenitic stainless steel specimens at low crosshead speeds (833.3 nm/s–9.8 nm/s) as shown in Figs. 5 and 6. This type of fracture can be attributed to the high hydrogen concentration on the cleavage plane of (100) owing to pile – up of hydrogen laden dislocations at this plane [17]. The extent of this fracture was observed to

increase with lowering in crosshead speed. At the lowest crosshead speed used (83.3 nm/s and 9.8 nm/s), cleavage fracture was observed to extend over the all fracture surfaces. In addition, intergranular fracture began to appear owing to availability of hydrogen due to long time to failure at these crosshead speeds.

Fracture surfaces for more stable 310 austenitic stainless steel specimens exhibited intergranular and quazi cleavage types of fracture at the lowest crosshead speed of 9.8 nm/s as shown in Figs (8 and 9). This result shows that even more stable austenitic stainless steel, with high SFE, can be embrittled when high hydrogen concentration is introduced to the sample. This type of fracture was not reported earlier and can be attributed to the severity of the embrittlement test. High hydrogen concentration changes the slip mode from easy cross slip to coplanar motion, which in turn makes dislocations bearing hydrogen to pile-up at the grain boundaries or any other obstacles to the dislocations movement, and increases the hydrogen concentration at these locations [17].

The effect of stability of austenitic stainless steel on the susceptibility to hydrogen embrittlement can be attributed to the differences in the austenite stability, which can be calculated using the emperical formula by Gladman *et al* [18].

$$Md_{30}(C) = 497 - 462(C+N) - 9.2(si) - 8.1(Mn) - 13.7(cr) - 20(Ni) - 18.5(Mc)$$

Utilizing the above formula shows that 304 austenitic stainless steel has Md_{30} above room temperature and its austenite phase is unstable and can be transformed to martensitic phases α^- and ε in presence of hydrogen [3, 9]. In contrast, more stable 310 austenitic stainless steel has more stable austenite phase and will only transform to ε phase owing to its very low Md_{30}. The presence of α^--martensite phase in less stable 304 austenitic stainless steel greatly enhances the hydrogen diffusivity owing to high hydrogen diffusivity of ferrite phase (bcc) structure [19] (10^{-8} cm^2/s) compare to only (10^{-12} cm^2/s) for austenite phase (fcc) structure [10].

The other important factor which controls the susceptibility of austenitic stainless steel to hydrogen embrittlement is the stacking fault energy (SFE) for the tested alloy [7]. The SFE of an alloy determines whether cross slip or coplanar motion is predominant. It is extensively reported in the literature that the hydrogen embrittlement of austenitic stainless steel resulted from lowering in SFE by absorbed hydrogen [8, 20]. Lowering in SFE energy leads to changes in slip mode, from easy cross slip to coplanar motion. Coplanar motion occurs in materials with low SFE and leads to dislocation pile-up at obstacles [7]. In the region of pile-up the hydrogen concentrations would be high.

In the current work, the stacking fault energy (SFE) for tested steels were measured using Schramm and Reed formula [21].

$$SFE\,(mJ/m2) = -53 + 6.2(Ni) + 0.7(cr) + 3.2(Mn) + 4.3(Mo)$$

The calculated values are 18 mJ/m^2 and 93 mJ/m^2 respectively for 304 and 310 austenitic stainless steels. This wide differences in the SFE values explain the differences in the susceptibility of these two steels to hydrogen embrittlement.

Surface cracks were observed on the surface of the annealed, sensitized and cold worked specimens. Intergranular cracks were observed and can be attributed to the action of hydrogen and the tensile test. Transgranular cracks were observed to propagate along or parallel to the slip bands as shown in Fig. 10. These cracks were observed by others and suggested to propagate along (110) and (111) planes [22, 23, 24]. This type of fracture may correspond to the fracture through the ε phase [23] or along ε/γ interface [23], since s phase forms in both alloys and has (111) habit plane.

Less cracking was observed in 12% cold worked 304 austenitic stainless steel compare to non cold worked specimens as can be seen by comparing Fig. 10 with Fig. 11. This can be attributed to the pre-existing of α martensite in the surface of cold worked specimens which may provide a rapid path for hydrogen to diffuse away from the specimen surface [25]. Thus preventing the build up of the critical concentration of hydrogen thought to be necessary for the formation of the expanded phases (γ^* and ε^*) [25, 26].

The surface of both 5 h and 24 h sensitized specimens exhibited more transgranular cracks than those on the surface of annealed specimens when the test was carried out at low crosshead speed as can be seen in Figs 12 and 13. This results can be attributed to the high content of martensite phases in sensitized specimens. These phases (α^- and ε) can act as crack initiation site or/and active path for hydrogen diffusion [10].

Specimens sensitized for 24 h showed more transgranular cracks and grain spall off compared to that for 5 h sensitized specimens. This result can be attributed to the embrittlement severity for 24 h sensitized specimens resulted from continuous precpitation of carbides and presence of high percentage of α^- martensite.

CONCLUSION

1. Less stable 304 austenitic stainless steel specimens exhibited both intergranular and transgranular

types of fracture mode when the test was carried out at low crosshead speeds of 83.3 nm/s and 9.8 nm/s.

2. 12% Cold worked 304 austenitic stainless steel specimens exhibited similar fracture morphology to that observed for non cold worked specimens over the most crosshead speed used.

3. Fracture surface of 5 h sensitized 304 austenitic stainless steel specimens exhibited cleavage fracture over all crosshead speeds used. However, intergranular fracture was the predominant fracture mode for 24 h sensitized specimens at low crosshead speeds of 83.3 nm/s and 9.8nm/s.

4. The extent of intergranular fracture insensitized specimens was observed to depend on both sensitization time and crosshead speed used.

5. More stable austenitic stainless steels can be embrittled in presence of high hydrogen fugacity.

6. Fracture surface of more stable 310 austenitic stainless steel exhibited both intergranular and quazi cleavage types of fracture node when tested at the lowest crosshead speed of 9.8 nm/s.

7. The results obtained in this work, support the observation of less surface cracking in hydrogen embrittled cold worked 304 austenitic stainless steel.

ACKNOWLEDGEMENT

I would like to express my sincere thanks to the Petroleum Research Centre for the Financial support while carrying out this work. Thanks are also extended to Professor John C. Scully at Leeds University, England for his constant interest and encouragement during the course of this work.

REFERENCES

[1] Vennett, R.M. and Ansell, G.S., 1969, Trans. ASM, 62, pp. 1007–1013.
[2] Benson, R.B., Dann, R.K. and Roberts, L.W., 1968, Trans AIME, 242, pp. 2199–2205.
[3] Holzworth, M.L. and Louthan, M.R., 1968, Corrosion, 24, pp. 110–124.
[4] Thompson, A.W., 1974, Hydrogen in Metals, I.M. Bernstein and A.W. Thompson eds., pp. 91–102, ASM, Cleveland, OH.
[5] Menta, M.L. and Burke, J., 1975, Corrosion, 31, pp. 108–110.
[6] Vaughan, D.A., Phalen, D.L., Beterson, C.L. and Boyd, W.K., 1963, Corrosion, 19, pp. 315t–325t.
[7] Odegard, B.C., Brooks, J.A. and West, J.A., 1976, Effect of Hydrogen on Behaviour of Materials, (A.W. Thompson and J.M. Bernstien eds.), pp. 631–641, AIME, New York, NY.
[8] Louthan, M.R. Caskey, G.R. Donovan, J.A. and Rawl, P.E., 1972, Mater. Sci. Eng., 10, pp. 357–368.
[9] Holzworth, M.L., 1969, Corrosion, 25, pp. 107–115.
[10] Tien, J.K., Thompson, A.W., Bernstien, I.M. and Richardson, R.V., 1976, Metall. Trans., 7A, pp. 821–829.
[11] Zheng, W. and Hardie, D., 1991, Corrosion Science, 32, pp. 23–26.
[12] Hannien, H. and Hakkarainen, T., 1980, Corrosion, 36, pp. 97–51.
[13] Briant, C.L., 1978, Metall. Trans., 9A, pp. 731–733.
[14] Briant, C.L., 1978, Scripta Met., 12, pp. 541–542.
[15] Hannula, S.P. Hanninen, H. and Tahtinen, S., 1984, Metall. Trans., 15A, pp. 2265–2211.
[16] Caskey, G.R., 1977, Scripta Met., 11, pp. 1077–1083.
[17] West, J.A. and Louthan, M.R., 1974, Metall. Trans., 10A, pp. 1675–1682.
[18] Pickering, F.B., Physical Metallurgy and the Design of Steels, Applied Science, Publishers Ltd., London, 1978, p. 229.
[19] Lange, K.W. and Konig, H.J., Proc. Second Int. Conf. on Hydrogen in Metals, 1977, p. 1A5, Pergamon, New York.
[20] Hartson, J.D. and Scully, J.C., 1970, Corrosion, 20, pp. 387–395.
[21] Schramm, R.E. and Reed, R.P., Metall. Trans., 6A, pp. 1345–1351.
[22] Liu, R., Narita, N., Altstetter, C.J., Birnabaum, H.K., 1980, Metall. Trans., 11A, pp. 1563–1574.
[23] Narita, N., Altstetter, C.J. and Birnabaum, H.K., 1982, Metall. Trans., 13A, pp. 1355–1365.
[24] Eliezer, D.E., Chakkrapani, D.G., Altstetter, C.J. and Pugh, E.N., 1979, Metall. Tans., 10A, pp. 935–941.
[25] Bently, A.P. and Smith, G.C., 1986, Scripta Met., 20, pp. 729–732.
[26] Bently, A.P. and Smith, G.C., 1986, Metall. Trans., 17A, pp. 1593–1600.